APL Photonics

Observation of gain-pinned dissipative solitons in a microcavity laser

Cite as: APL Photonics **5**, 086103 (2020); https://doi.org/10.1063/5.0010633
Submitted: 13 April 2020 . Accepted: 19 July 2020 . Published Online: 04 August 2020

M. Pieczarka, D. Poletti, C. Schneider, S. Höfling, E. A. Ostrovskaya, G. Sęk, and M. Syperek

Observation of gain-pinned dissipative solitons in a microcavity laser

Cite as: APL Photon. 5, 086103 (2020); doi: 10.1063/5.0010633
Submitted: 13 April 2020 • Accepted: 19 July 2020 •
Published Online: 4 August 2020

M. Pieczarka,[1,2,a)] D. Poletti,[3,4] C. Schneider,[5] S. Höfling,[5,6] E. A. Ostrovskaya,[2] G. Sęk,[1] and M. Syperek[1]

AFFILIATIONS

[1]Department of Experimental Physics, Wrocław University of Science and Technology, Wyb. Wyspiańskiego 27, 50-370 Wrocław, Poland
[2]ARC Centre of Excellence in Future Low-Energy Electronics Technologies and Nonlinear Physics Centre, Research School of Physics, The Australian National University, Canberra, ACT 2601, Australia
[3]Science and Math Cluster, Singapore University of Technology and Design, 8 Somapah Road, 487372, Singapore
[4]EPD Pillar, Singapore University of Technology and Design, 8 Somapah Road, 487372, Singapore
[5]Technische Physik and Wilhelm-Conrad-Röntgen-Research Center for Complex Material Systems, Universität Würzburg, Am Hubland, 97074 Würzburg, Germany
[6]SUPA, School of Physics and Astronomy, University of St. Andrews, St. Andrews KY16 9SS, United Kingdom

[a)]**Author to whom correspondence should be addressed:** maciej.pieczarka@pwr.edu.pl

ABSTRACT

We demonstrate an experimental approach for creating spatially localized states in a semiconductor microcavity laser. In particular, we shape the spatial gain profile of a quasi-one-dimensional microcavity laser with a nonresonant, pulsed optical pump to create spatially localized structures, known as gain-pinned dissipative solitons, that exist due to the balance of gain and nonlinear losses. We directly probe the ultrafast formation dynamics and decay of these localized structures, showing that they are created on a picosecond timescale, orders of magnitude faster than laser cavity solitons. All of the experimentally observed features and dynamics are reconstructed by numerical modeling using a complex Ginzburg–Landau model, which explicitly takes into account the carrier density dynamics in the semiconductor.

I. INTRODUCTION

The past decades of research in nonlinear optics have uncovered an immense variety of systems and material configurations that can support optical solitons.[1] In conservative optical systems, temporal or spatial solitons are supported by a nonlinearity compensating for the dispersion or diffraction of light in the propagating geometry.[2–4] The real-world photonic devices suffer from intrinsic losses, and it is essential to achieve the balance not only between the dispersion or diffraction and the nonlinearity but also in the energy flow, i.e., between the gain and loss in the system, to support self-localized structures.[5] Spatially localized dissipative structures, called cavity solitons,[6] have been successfully created in broad area vertical cavity surface emitting lasers (VCSELs).[7] In this configuration, the device is kept below the lasing threshold, while the use of an additional external coherent holding laser beam is set up to achieve an optical bistability condition leading to the creation of stable localized modes. Their control is implemented with an additional writing laser beam or a pulse.[8,9] The spatially localized cavity solitons are not created in a propagating geometry in the device, but are confined within the optical microcavity mirrors and can be moved in the transverse direction (perpendicular to the cavity). In the scheme most suitable for applications, the broad-area microcavity is driven above the threshold and is coupled to an external cavity mirror or to a saturable absorber, which allows for the creation of a stable cavity soliton laser.[10–12]

When a laser is driven above the threshold, the spatially uniform gain without an additional coherent holding beam (or other source of bistability) is not capable of sustaining a strongly localized bright mode that becomes unstable due to the action of the

gain outside of its core.[13] Therefore, a different approach has to be implemented to overcome the competition between the coherent holding beam and the gain of the lasing field. One can imagine modifying the spatial gain profile in the device to tackle this issue. A straightforward way would be to contain gain in a small spatial volume, while the loss outside of this "hot-spot" provides a balance between gain and loss around the bright soliton core.[14]

Dissipative modes pinned by a localized gain have been intensively studied theoretically, and their realizations in various systems were proposed.[15] These localized structures, known as gain-pinned dissipative solitons, have been predicted to be robust and stable over a wide range of parameters even in the absence of Kerr nonlinearity in the material. In particular, a one-dimensional complex Ginzburg–Landau model with an infinitesimally localized gain in a dissipative medium supports an exact dissipative soliton solution,[15,16]

$$E(x) = A\sinh(\kappa(|x| + \xi))^{(-1+i\mu)}, \quad (1)$$

where A is the amplitude of the mode, μ is the chirp coefficient, and κ, ξ determine the shape of the field envelope function. It is not a generic solution, as the analytical form is only available under a constraint on the parameters. Nevertheless, it has been shown numerically that this type of solution represents a broader family of stable localized modes.[16] The gain-pinned dissipative soliton solution, Eq. (1), is an attractor[15,16] of the complex Ginzburg–Landau model and is independent of initial conditions (see the supplementary material for numerical examples). Moreover, the gain-pinned dissipative solitons are expected to be stabilized in systems with non-negligible nonlinear losses[15,16] or in the absence of nonlinear losses in a system with cubic gain.[17]

The shapes of gain-pinned dissipative solitons are shown in Fig. 1(a). In the simplest case of linear losses in the cavity, without Kerr nonlinearity, the mode profile is trivial and is characterized by an exponential decay outside of the gain spot [black lines in Fig. 1(a)].[14,15] However, the shape is considerably changed when nonlinear losses are present in the system (two-photon absorption), localizing the mode around the "hot-spot" [green lines in Fig. 1(a)].

The spatial profile of a dissipative soliton [Eq. (1)] is dictated by the balance between gain and loss.[1,15] The mode profile can be written in a generalized form as $E(x) = A(x)e^{i\phi(x)}$ with the local amplitude $A(x)$ and the phase $\phi(x)$. The local energy flux $j(x) = A^2(x)\frac{d\phi(x)}{dx}$ and its derivative $g(x) = \frac{dj(x)}{dx}$ can be used to quantify the local gain $g(x) > 0$ and loss $g(x) < 0$. The numerically calculated gain-pinned dissipative soliton profile $|E(x)|^2$ and $j(x)$, $g(x)$ (taking a finite gain spot) are shown in Fig. 1(b). The gain-pinned dissipative soliton is associated with the characteristic spatial profiles of these quantities. Specifically, the energy flux $j(x)$ is zero at the soliton center, negative on the left, and positive on the right, reflecting the energy outflow from the center to the tails of the mode. The local energy gain $g(x)$ is positive in the center, where the gain spot is located, and negative outside, indicating energy loss. The gain–loss balance criterion can be expressed as $\int_{-\infty}^{+\infty} g(x)dx = 0$ and is fulfilled for the gain-pinned dissipative soliton.[1,14–16]

In this work, following the existing theoretical proposals, we present the *proof-of-concept* experimental realization of spatially localized structures, which are interpreted as gain-pinned spatial dissipative solitons, in the quasi-one-dimensional semiconductor microcavity schematically shown in Fig. 2(a). We shape the gain spot by shining a focused, pulsed laser beam tuned above the bandgap of the cavity material (GaAs) to generate a dissipative soliton that is strongly localized in space and decays in time. The observed lasing mode is confined around the area of the resolution-limited gain. The ultrafast dynamics of the soliton formation and decay, the evolution of the spatial profile, and the far-field (the in-plane momentum spectrum) emission are probed directly by streak camera measurements. The gain-pinned solitons form on a timescale of a few picoseconds, which is orders of magnitude faster than the previously reported cavity soliton manipulation dynamics[8,9,12,18] and is comparable to optically injected bright exciton–polariton soliton timescales.[19] We successfully reconstruct all the observed dynamical features by employing a complex Ginzburg–Landau model.

II. SAMPLE AND EXPERIMENTAL SETUP

Starting from a planar GaAs VCSEL sample, the quasi-one-dimensional cavity structures are processed via electron beam lithography and etched using electron cyclotron-resonance reactive-ion-etching in the form of stripes of hundreds of micrometers in length and only a few micrometers in width, creating an effectively one-dimensional transverse confinement of optical modes. The planar sample is an AlAs/GaAs $\lambda/2$-long planar microcavity composed of two distributed Bragg reflectors (DBRs) enclosing two stacks of four $In_{0.3}Ga_{0.7}As$/GaAs quantum wells (QWs) located at the antinodes of the photon field. The ground state of the quantum well is located around 1.262 eV at cryogenic temperatures. The measured microcavity Q-factor was about 1000 before etching. The sample is characterized with a substantial disorder potential,[20] pronounced after etching (see the supplementary material, Sec. II B). The possible origin of disorder is the strong fluctuations and strain induced by the high indium content QWs grown

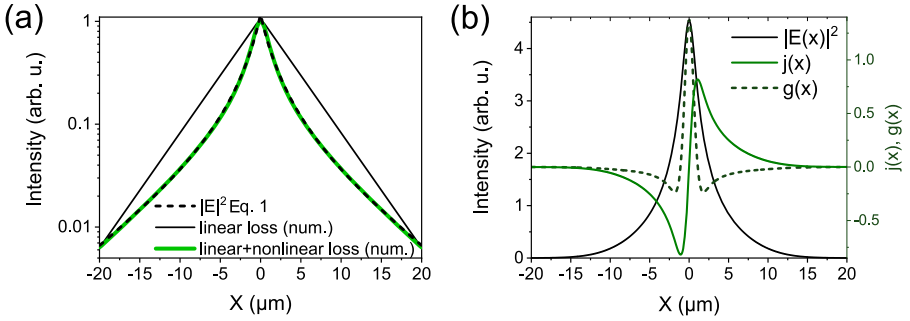

FIG. 1. (a) Gain-pinned dissipative soliton shapes calculated numerically with a constant (CW) linear pump of finite width under the assumption of linear (black lines) and nonlinear losses (green lines) in the system, and the analytical expression from Eq. (1) is plotted with a dashed line. (b) Dissipative soliton profile $|E(x)|^2$ plotted with the local energy flux $j(x)$ and the local energy generation $g(x)$ characterizing the gain–loss distribution of the mode.

near the critical thickness.[21] This contributes to the inhomogeneous broadening of the laser emission below the threshold [Fig. 2(c)]. Additional linewidth broadening of the emission from quasi-one-dimensional stripes is induced by the imperfections of the sidewalls of the fabricated structures.

The localized gain is provided by a pulsed laser source (Ti:sapphire, 140 fs pulses with a 76 MHz repetition rate), frequency-tuned above the GaAs bandgap and to one of the reflectivity minima of the cavity for the efficient photo-excitation of electron–hole pairs. The laser spot is focused via an objective (NA = 0.42) on the surface of the cavity laser stripe to a Gaussian spot of 1.5 μm full width at half maximum (FWHM) (see the supplementary material, Sec. II G). In contrast to typical GaAs-based waveguide designs for optical soliton experiments, where the detrimental effects of nonlinear losses are kept to a minimum,[3,4] our sample design places the fundamental cavity mode in the spectral range where the nonlinear refractive index is small and defocusing and, most importantly, where significant nonlinear losses due to the two-photon absorption are expected to occur[22] (see parameter calculation in the supplementary material, Sec. II E). These material characteristics provide the conditions for the generation of gain-pinned dissipative solitons, as indicated by theoretical models.[15] Additionally, the nonlinear loss channel is known to be more pronounced in photonic devices due to a small volume of the confined photon mode,[23–26] effectively lowering the total power densities at which the nonlinear effects occur. This property makes our system most suitable for exploiting the nonlinear loss in the process of dissipative soliton formation.

In the experiment, the sample is kept in a continuous flow liquid helium cryostat at a temperature T = 5 K. The emission from the sample is collected via the microscope objective in the reflection setup configuration and then further transferred through a set of achromatic lenses to a spectrometer for a near-field (real space) and far-field (momentum space) imaging. The monochromator (0.5 m focal length, Princeton Instruments) outputs are coupled to a two-dimensional InGaAs near-infrared camera (NIRvana Princeton Instruments) and to a Hamamatsu streak camera (temporal resolution of about 3 ps). For imaging purposes, the monochromator grating is set to the zeroth-order mode.

III. RESULTS

The power dependent measurements of the output intensity of the device luminescence reveal a typical lasing threshold (where

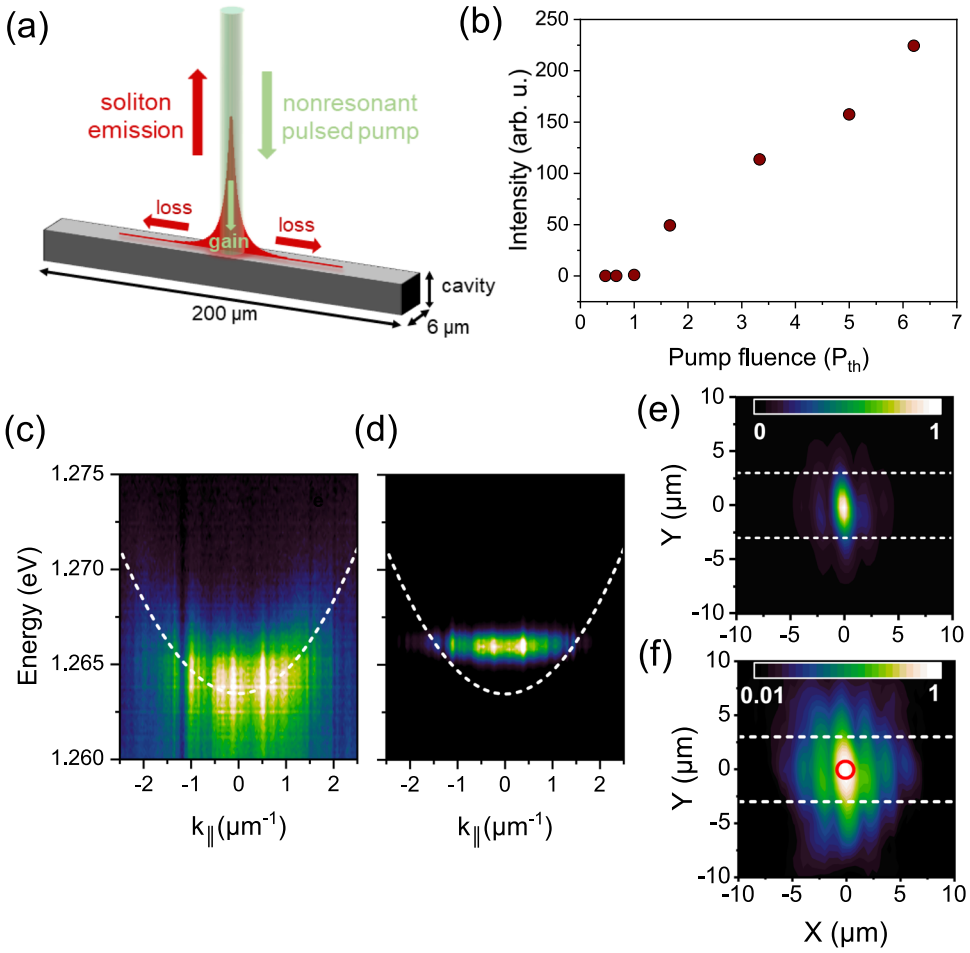

FIG. 2. (a) Schematics of the experimental realization. The dimensions of the microlaser stripe are indicated in this figure. (b) Power dependent input–output series of an investigated microcavity laser showing a typical threshold behavior. [(c) and (d)] Far-field spectra of the lasing mode (c) below and (d) at the lasing threshold. $k_{\parallel}$ is the in-plane wavevector along the stripe. The dashed line indicates the cavity photon momentum dispersion. Real-space images of the spatial shape of the dissipative soliton for $P = 3.3P_{th}$ in linear (e) and in logarithmic (f) color scales. The red circle indicates the gain spot.

the lasing threshold value P_{th} = 29 pJ/μm^2), see Fig. 2(b), being accompanied by the emission linewidth narrowing and the distinct blueshift of the emission energy (by about 3 meV), as seen in the far-field spectra in Figs. 2(c) and 2(d). This energy shift originates from the local cavity refractive index change due to the free carriers generated in the GaAs spacer of the cavity volume by a nonresonant pump pulse.[25,27] Subsequently, carriers relax to the quantum wells, creating an electron–hole plasma, and provide gain for the lasing and the localized mode pinning. The broad momentum range of the far-field spectrum in Fig. 2(d) reflects the strong localization observed in the real space, as shown in Figs. 2(e) and 2(f). The spatial extent of the localized structure is constrained to the diffraction-limited gain spot (~1.5 μm) in the direction along the long axis of the stripe, and the sample dimensions in the direction of the short axis (mode width is about 4 μm in the perpendicular direction). The mode volume can possibly be confined to an even smaller area by employing narrower microwire cavities or photonic crystal nanocavities.[24]

The pulsed excitation used in the experiment results in a non-stationary, decaying gain and lasing of the localized structure owing to the finite lifetime of the excited carriers and cavity photons in the system. Hence, we perform an analysis of the shape and intensity of the gain-pinned localized structure in the direct time-resolved experiment. The dynamics of the near and far-field emission patterns along the microcavity stripe excited above the lasing threshold are shown in Figs. 3(a)–3(c) with the analysis of the spatial width and the signal intensity shown in Fig. 3(d). Importantly, this dynamics occurs on the timescale of ~10^2 ps, which is *three orders of magnitude* longer than the timescale of the pulsed excitation (~10^2 fs). One distinguishes three stages in the dynamics. First, the pump pulse creates high-energy electrons and holes in the barrier, which relax and form a gain medium within the quantum well states [stage I in Fig. 3(d)]. Then, after about 10 ps, the localized lasing occurs with the rapid narrowing of the spatial width down to the optical resolution limit of the setup (of ~1.5 μm) in stage II. Subsequently, the emission pulse maintains its narrow width with the strongest emission of photons, and eventually, it decays and spreads at later times (after t > 60 ps), which is evidenced in the increase of the spatial width, stage III in Fig. 3(d). This latter stage is the linear regime, where the gain decays and the nonlinearity is too weak to sustain the localized shape. The onset of the nonlinearly localized structure is characterized by an ultra-short time of ~3 ps, being limited by the temporal resolution of the setup. The observed fast response is a result of the onset of the stimulated emission and the ultrafast dynamics of electronic semiconductor nonlinearities occurring on the timescales of a few picoseconds.[25,28–30]

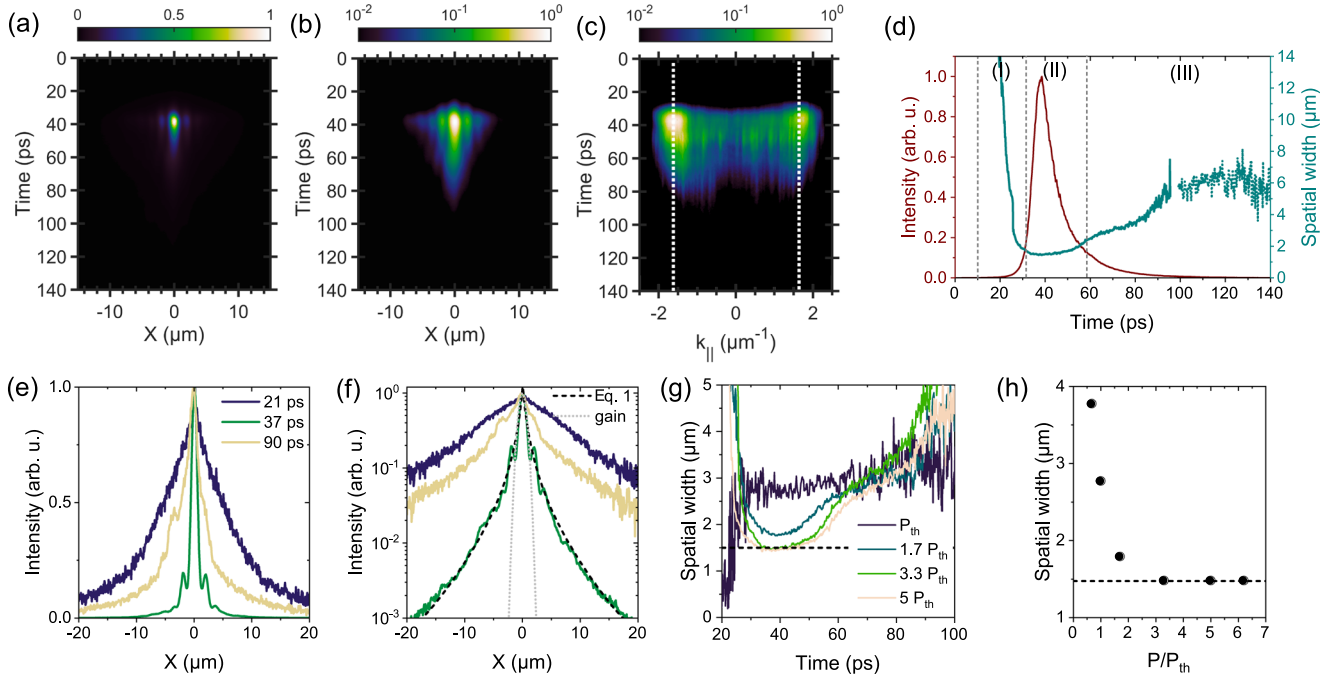

FIG. 3. [(a) and (b)] Measured time-resolved spatial dynamics of the spatial emission in (a) linear and (b) logarithmic color scales, respectively, at pumping power $P = 3.3P_{th}$. (c) Far-field dynamics, where two distinct wavevectors are visible and indicated with white dotted lines. (d) Time dependency of the signal intensity and its spatial width [full width at half maximum (FWHM)] following the 140 fs excitation pulse. Three different stages in the time dynamics are indicated in this figure. The region with a low signal-to-noise ratio of the spatial width data is depicted with a dotted line. [(e) and (f)] Spatial distributions of the emission at different times are indicated in these figures. The dashed curve is the gain-pinned dissipative soliton envelope curve [Eq. (1)] fitted to the experimental data $|E(x)|^2$. The gray dotted line indicates the Gaussian gain spot. (g) Spatial localization dynamics under different pumping powers showing the decrease in the spatial width with increasing number of photons and gain in the system. (h) Minimal spatial width of the structure, showing typical density-dependent narrowing of the structure width. Dashed lines in (g) and (h) indicate the spatial resolution of the setup.

The three characteristic regimes in the dynamics are also reflected in the spatial shape of the emission, as shown in Figs. 3(e) and 3(f). At the onset of lasing, when the emission intensity is low, the lasing mode is weakly localized around the gain spot with a characteristic spatial exponential decay. Subsequently, the lasing intensity rises, reaching a maximum at around $t = 37$ ps, whereby the nonlinear localization and formation of a strongly localized mode occur. The spatial profile of the localized structure, see Fig. 3(f), reveals the gain-pinned soliton solution shown in Fig. 1 and follows the analytical expression of Eq. (1). The strong spatial focusing is caused by the presence of nonlinear losses in the system since any other nonlinearities (e.g., due to the Kerr effects and excitonic nonlinearity; see the supplementary material, Sec. II E) are defocusing and would lead to a trivial broadened shape, similar to the one in the linear regime in Fig. 1(a). The observed self-focusing is a proof that the device operates in the weak coupling regime because the exciton–polariton interactions in the strong coupling regime would result in a strongly defocusing nonlinearity. Additionally, one can safely rule out the thermal effects, which have much longer timescales (microseconds) and manifest themselves in a redshift of the cavity mode energy.[31]

The far-field spectrum contains two distinct peaks [Fig. 3(c)] due to the outward propagation of photons from the gain spot. This shape is the consequence of a dynamical balance of the energy flow characteristic of dissipative solitons, as discussed in the Introduction;[1,14,15] see Fig. 1(b). Additionally, backscattering of these propagating waves on the intrinsic disorder of the sample causes the characteristic interference pattern observed on top of the localized structure. This effect is seen both in time integrated, Fig. 2(f), and time-resolved images, Fig. 3(b). The disorder scattering in the sample adds a small spatial modulation to the shape described by Eq. (1), the latter being independent of the particular position on the sample (see the supplementary material for data taken at a different laser cavity stripe). At longer times after the excitation pulse, the nonlinear localization weakens and the mode once again displays exponentially decaying tails with additional disorder-induced modulation. The nonlinear localization mechanism of the dissipative structure is confirmed in the density-dependent measurements, where one observes sharp narrowing of the spatial width above the lasing threshold, as shown in Figs. 2(g) and 2(h). The minimum measured spatial width is due to the setup resolution, being also the limitation for the gain spot diameter, and is indicated by a horizontal dashed line in Figs. 2(g) and 2(h). We note that no localization is observed when the microcavity is pumped with a large quasi-homogeneous pump spot of about 40 μm, which rules out the localization caused by the spatial hole burning effect or trivial localization by the local disorder (see the supplementary material, Sec. II C).

IV. NUMERICAL SIMULATIONS

To verify the interpretation of the experiment proposed above, we perform numerical simulations based on a complex Ginzburg–Landau equation including nonresonant pumping and dissipation in the system, taking into account the nonlinear losses and simplified dynamics of the photo-excited reservoir of carriers. The electric field envelope $E(x, t)$ is coupled to a rate equation for the density of the carrier reservoir $N(x, t)$, i.e., the gain medium,

$$\frac{\partial}{\partial t}E(x,t) = \frac{ic^2}{2k_c n_c^2}\frac{\partial^2}{\partial x^2}E(x,t) + \frac{1}{2}\left(\Gamma N(x,t) - \gamma_c - \beta|E(x,t)|^2\right)E(x,t) - iV(x)E(x,t) - i\alpha N(x,t)E(x,t), \quad (2)$$

$$\frac{\partial}{\partial t}N(x,t) = P(x,t) - \gamma N(x,t) - \Gamma|E(x,t)|^2 N(x,t). \quad (3)$$

Here, the cavity photons are described by an effective mass along the microcavity stripe $m = E_c n_c^2/c^2$, where $E_c = \hbar k_c c$ is the cavity photon energy at $k_{\|} = 0$, n_c is the cavity refractive index, c is the speed of light, and k_c is the confined longitudinal mode wavenumber. The gain in the system is described by the coefficient Γ, and the linear loss (cavity photon lifetime) is denoted by γ_c. The nonlinear losses (e.g., two-photon absorption) in the system are denoted by β. The carrier reservoir decay rate is determined by γ. The nonresonant pumping of the system is described by the rate of injection of the carrier density $P(x, t)$. This term can be constant for continuous wave (CW) simulations or can be expressed as $P(x)\delta(t = 0)$ for the ultrafast pulsed excitation corresponding to the experimental conditions, setting the initial spatial density distribution of carriers in the microcavity. Local modifications of the cavity refractive index are introduced through the carrier density and scaled with the linewidth enhancement factor parameter α. The material disorder is described as a static potential $V(x)$ (see the supplementary material, Sec. II B). In the case of CW excitation (e.g., Fig. 1), the model can be reduced to a single equation under the assumption of the carrier density $N(x, t)$ adiabatically following the field evolution $|E(x, t)|^2$. In this case, Eq. (3) can be solved for a CW pump $P(x, t) = P(x)$ (see the supplementary material, Sec. I A)

$$N(x,t) = \frac{P(x)}{\gamma + \Gamma|E(x,t)|^2}. \quad (4)$$

As shown in Fig. 4, our numerical simulations successfully reconstruct all the characteristic features seen in the experiment, namely, the shape of the localized structure and its dynamics in the real space as well as the far-field spectra. As shown in Fig. 4(a), the dissipative structure is localized around the gain spot in real space, and its Fourier spectrum contains two main wavevector components, as shown in Fig. 4(c). Power-dependent simulations yield the narrowing of the spatial width, see Fig. 4(f), which is the manifestation of the nonlinear trapping mechanism seen in the experiment, as shown in Fig. 3(h). Inclusion of nonlinear losses in the model is essential for reproducing the experimental shape of the soliton, as the model with only linear losses captures neither the dynamics shown in Fig. 3 nor the spatial width narrowing (additional numerical results are presented in the supplementary material, Sec. I). Our model also includes a random disorder potential (caused by variations of the refractive index or imperfections of the thickness of the fabricated microwire) with similar characteristics to the one measured experimentally, which slightly modulates the shape. The shape of the dissipative localized structure is found to be robust to the change of the particular realizations of the disorder, which are kept within the experimentally measured values.

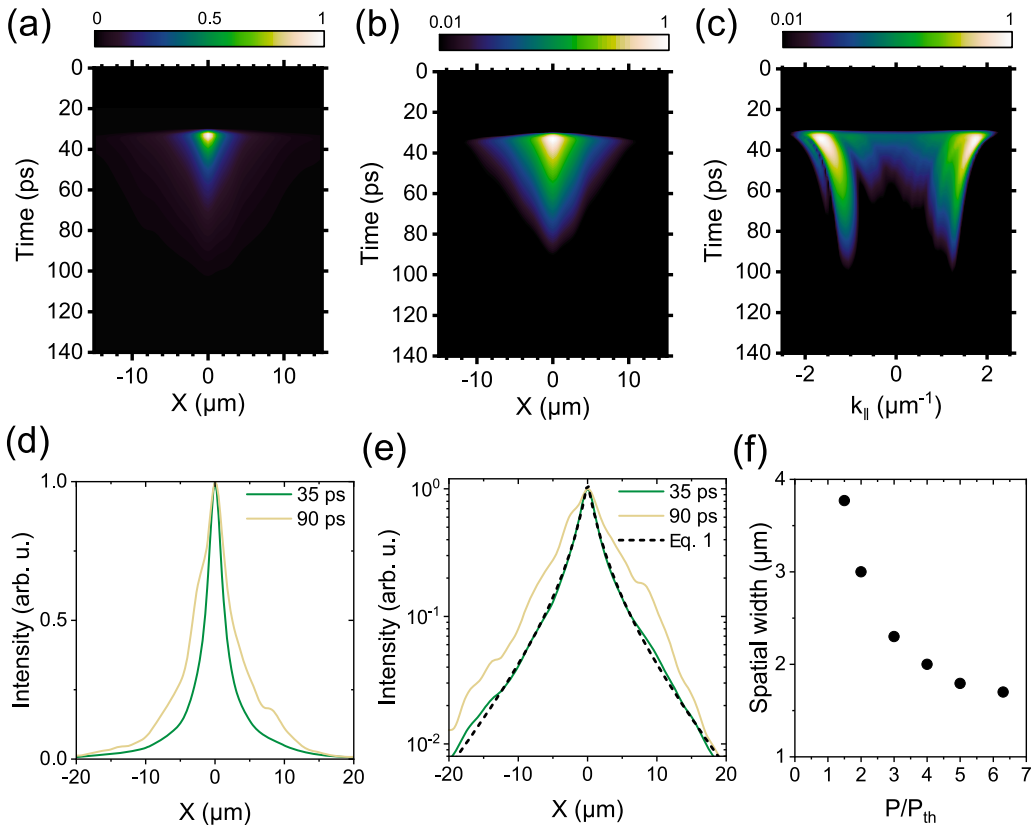

FIG. 4. [(a) and (b)] Simulated dynamics of the localized structure emission in (a) linear and (b) logarithmic color scales. (c) Far-field dynamics. [(d) and (e)] Spatial distributions at two different times: presenting the localized structure at 35 ps and the diffracted distribution at a later time 90 ps, with the intensity plotted on the (d) linear and (e) logarithmic scale. Analytical fit of the gain-pinned dissipative soliton profile, Eq. (1), at 35 ps is drawn with a dashed line. (f) Narrowing of the spatial width with pump amplitude limited by the width of the simulated gain spot. Simulation parameters are $\gamma_c = 1$ ps^{-1}, $\gamma = 1$ ns^{-1}, $m^* = 3.12 \cdot 10^{-5}$ m_0, where m_0 is the free electron mass, $\Gamma = 0.01$ μm/ps, $\beta = 1$ μm/ps, and $\alpha = 4.6 \cdot 10^{-3}$ μm/ps.

V. CONCLUSIONS

We have demonstrated experimentally one-dimensional localized dissipative structures, which have the predicted properties of gain-pinned dissipative solitons. We demonstrate these structures in a GaAs-based VCSEL for which (i) the experimental realization is particularly convenient due to nonresonant pumping, above the active material bandgap; (ii) the structure size is limited by the gain profile and is, therefore, much smaller than the typical VCSEL solitons[7,8,10,12] and comparable to the size of exciton–polariton bright solitons;[19,32] and (iii) the onset dynamics, being driven by stimulated laser emission, is an ultra-fast process in the range of single picoseconds, orders of magnitude faster than cavity solitons[9,18] and of the same order of magnitude as bright exciton–polariton solitons.[19,33] The temporal decay of the lasing signal observed in our experiment is due to the pulsed regime of excitation, whereby the gain-pinned dissipative soliton is created in a dynamical "single-shot" regime. However, the strongly localized dissipative structures persist on the timescales exceeding the timescale of the pulsed excitation by several orders of magnitude. This long timescale is determined by the lifetime of the gain medium injected by the pulse in the experiment. Continuous wave (CW) pumping would be capable of maintaining steady-state soliton lasing with a constant gain. This offers a possibility to create stable, steady-state gain-pinned dissipative solitons localized in a semiconductor device.

Although our study explores a quasi-one-dimensional version of a VCSEL, our results pave the way toward creating stable two-dimensional solitary modes, which, as predicted theoretically,[34] are within reach in modern semiconductor microcavities of a similar design. Manipulation of the soliton position and its transversal propagation can be performed by the spatial modulation of the excitation beam, using spatial light modulators (SLMs), offering exciting possibilities for the creation of two-dimensional vortex solitons[34–37] or multi-soliton structures.[38,39] Furthermore, gain-pinned dissipative solitons presented here, due to their robustness and simple realization, could be arranged into lattices. Their self-localization enables the realization of a dense array of solitons (small lattice constant arrangement) preventing the development of a broad lasing area far above the threshold. Therefore, gain-pinned solitons represent a perfect platform for simulations of classical Hamiltonians,[40,41] studies of complex topological ordering,[42,43] and spontaneous symmetry breaking in laser systems.[38,44,45]

SUPPLEMENTARY MATERIAL

See the supplementary material for additional experimental and numerical data supporting this work.

ACKNOWLEDGMENTS

M.P. would like to acknowledge stimulating discussions with Yuri S. Kivshar and Dragomir N. Neshev. Assistance by Fabian Langer, Monika Emmerling, and Adriana Wolf during sample fabrication is acknowledged. This work was supported by the National Science Center in Poland, by Grant Nos. 2016/23/N/ST3/01350 and 2018/30/E/ST7/00648, and by the Polish National Agency for Academic Exchange. The Würzburg group gratefully acknowledges support by the State of Bavaria. The work at the Australian National University was supported by the Australian Research Council.

DATA AVAILABILITY

The data that support the findings of this study are available from the corresponding author upon reasonable request.

REFERENCES

[1] *Dissipative Solitons: From Optics to Biology and Medicine*, Lecture Notes in Physics Vol. 751, edited by N. Akhmediev and A. Ankiewicz (Springer, Berlin, Heidelberg, 2008), p. 477.
[2] Z. Chen, M. Segev, and D. N. Christodoulides, "Optical spatial solitons: Historical overview and recent advances," Rep. Prog. Phys. **75**, 086401 (2012).
[3] H. S. Eisenberg, Y. Silberberg, R. Morandotti, A. R. Boyd, and J. S. Aitchison, "Discrete spatial optical solitons in waveguide arrays," Phys. Rev. Lett. **81**, 3383–3386 (1998).
[4] J. S. Aitchison, K. Al-Hemyari, C. N. Ironside, R. S. Grant, and W. Sibbett, "Observation of spatial solitons in AlGaAs waveguides," Electron. Lett. **28**, 1879 (1992).
[5] P. Coullet, "Localized patterns and fronts in non-equilibrium systems," Int. J. Bifurcation Chaos Appl. Sci. Eng. **12**, 2445–2457 (2002).
[6] T. Maggipinto, M. Brambilla, G. K. Harkness, and W. J. Firth, "Cavity solitons in semiconductor microresonators: Existence, stability, and dynamical properties," Phys. Rev. E **62**, 8726–8739 (2000).
[7] S. Barland, J. R. Tredicce, M. Brambilla, L. A. Lugiato, S. Balle, M. Giudici, T. Maggipinto, L. Spinelli, G. Tissoni, T. Knödl, M. Miller, and R. Jäger, "Cavity solitons as pixels in semiconductor microcavities," Nature **419**, 699–702 (2002).
[8] F. Pedaci, S. Barland, E. Caboche, P. Genevet, M. Giudici, J. R. Tredicce, T. Ackemann, A. J. Scroggie, W. J. Firth, G.-L. Oppo, G. Tissoni, and R. Jäger, "All-optical delay line using semiconductor cavity solitons," Appl. Phys. Lett. **92**, 011101 (2008).
[9] T. Elsass, K. Gauthron, G. Beaudoin, I. Sagnes, R. Kuszelewicz, and S. Barbay, "Fast manipulation of laser localized structures in a monolithic vertical cavity with saturable absorber," Appl. Phys. B **98**, 327–331 (2010).
[10] P. Genevet, S. Barland, M. Giudici, and J. R. Tredicce, "Cavity soliton laser based on mutually coupled semiconductor microresonators," Phys. Rev. Lett. **101**, 123905 (2008).
[11] Y. Tanguy, T. Ackemann, W. J. Firth, and R. Jäger, "Realization of a semiconductor-based cavity soliton laser," Phys. Rev. Lett. **100**, 013907 (2008).
[12] F. Gustave, N. Radwell, C. McIntyre, J. P. Toomey, D. M. Kane, S. Barland, W. J. Firth, G. L. Oppo, and T. Ackemann, "Observation of mode-locked spatial laser solitons," Phys. Rev. Lett. **118**, 044102 (2017).
[13] X. Hachair, F. Pedaci, E. Caboche, S. Barland, M. Giudici, J. R. Tredicce, F. Prati, G. Tissoni, R. Kheradmand, L. A. Lugiato, I. Protsenko, and M. Brambilla, "Cavity solitons in a driven VCSEL above threshold," IEEE J. Sel. Top. Quantum Electron. **12**, 339 (2006).
[14] D. A. Zezyulin, Y. V. Kartashov, and V. V. Konotop, "Solitons in a medium with linear dissipation and localized gain," Opt. Lett. **36**, 1200–1202 (2011).
[15] B. A. Malomed, "Spatial solitons supported by localized gain [Invited]," J. Opt. Soc. Am. B **31**, 2460 (2014); arXiv:1408.3579.
[16] C.-K. Lam, B. A. Malomed, K. W. Chow, and P. K. A. Wai, "Spatial solitons supported by localized gain in nonlinear optical waveguides," Eur. Phys. J.: Spec. Top. **173**, 233–243 (2009).
[17] O. V. Borovkova, V. E. Lobanov, and B. A. Malomed, "Stable nonlinear amplification of solitons without gain saturation," Europhys. Lett. **97**, 44003 (2012).
[18] X. Hachair, L. Furfaro, J. Javaloyes, M. Giudici, S. Balle, J. Tredicce, G. Tissoni, L. A. Lugiato, M. Brambilla, and T. Maggipinto, "Cavity-solitons switching in semiconductor microcavities," Phys. Rev. A **72**, 013815 (2005).
[19] M. Sich, D. N. Krizhanovskii, M. S. Skolnick, A. V. Gorbach, R. Hartley, D. V. Skryabin, E. A. Cerda-Méndez, K. Biermann, R. Hey, and P. V. Santos, "Observation of bright polariton solitons in a semiconductor microcavity," Nat. Photonics **6**, 50–55 (2012); arXiv:1109.1962.
[20] M. Pieczarka, M. Syperek, Ł. Dusanowski, A. Opala, F. Langer, C. Schneider, S. Höfling, and G. Sęk, "Relaxation oscillations and ultrafast emission pulses in a disordered expanding polariton condensate," Sci. Rep. **7**, 7094 (2017).
[21] B. Elman, E. S. Koteles, P. Melman, C. Jagannath, J. Lee, and D. Dugger, "*In situ* measurements of critical layer thickness and optical studies of InGaAs quantum wells grown on GaAs substrates," Appl. Phys. Lett. **55**, 1659–1661 (1989).
[22] M. Sheik-Bahae, D. J. Hagan, and E. W. Van Stryland, "Dispersion and band-gap scaling of the electronic Kerr effect in solids associated with two-photon absorption," Phys. Rev. Lett. **65**, 96–99 (1990).
[23] S. Combrié, A. De Rossi, Q. V. Tran, and H. Benisty, "GaAs photonic crystal cavity with ultra-high Q: Microwatt nonlinearity at 1.55 μm," Opt. Lett. **33**, 1908 (2008).
[24] M. Notomi and H. Taniyama, "On-demand ultrahigh-Q cavity formation and photon pinning via dynamic waveguide tuning," Opt. Express **16**, 18657 (2008).
[25] E. Yüce, G. Ctistis, J. Claudon, E. Dupuy, K. J. Boller, J.-M. Gérard, and W. L. Vos, "Competition between electronic Kerr and free-carrier effects in an ultimate-fast optically switched semiconductor microcavity," J. Opt. Soc. Am. B **29**, 2630 (2012).
[26] M. Soljačić and J. D. Joannopoulos, "Enhancement of nonlinear effects using photonic crystals," Nat. Mater. **3**, 211–219 (2004).
[27] A. A. Said, M. Sheik-Bahae, D. J. Hagan, T. H. Wei, J. Wang, J. Young, and E. W. Van Stryland, "Determination of bound-electronic and free-carrier nonlinearities in ZnSe, GaAs, CdTe, and ZnTe," J. Opt. Soc. Am. B **9**, 405 (1992).
[28] W. Xie, F.-K. Hsu, Y.-S. Lee, S.-D. Lin, and C. W. Lai, "Multiple-pulse lasing from an optically induced harmonic confinement in a highly photoexcited microcavity," Optica **3**, 1477 (2016).
[29] H. Altug, D. Englund, and J. Vučković, "Ultrafast photonic crystal nanocavity laser," Nat. Phys. **2**, 484–488 (2006).
[30] P. J. Harding, T. G. Euser, Y.-R. Nowicki-Bringuier, J.-M. Gérard, and W. L. Vos, "Dynamical ultrafast all-optical switching of planar GaAsAlAs photonic microcavities," Appl. Phys. Lett. **91**, 111103 (2007).
[31] S. Anguiano, A. A. Reynoso, A. E. Bruchhausen, A. Lemaître, J. Bloch, and A. Fainstein, "Three-dimensional trapping of light with light in semiconductor planar microcavities," Phys. Rev. B **99**, 195308 (2019).
[32] D. V. Skryabin, Y. V. Kartashov, O. A. Egorov, M. Sich, J. K. Chana, L. E. Tapia Rodriguez, P. M. Walker, E. Clarke, B. Royall, M. S. Skolnick, and D. N. Krizhanovskii, "Backward Cherenkov radiation emitted by polariton solitons in a microcavity wire," Nat. Commun. **8**, 1554 (2017).
[33] D. Tanese, H. Flayac, D. Solnyshkov, A. Amo, A. Lemaître, E. Galopin, R. Braive, P. Senellart, I. Sagnes, G. Malpuech, and J. Bloch, "Polariton condensation in solitonic gap states in a one-dimensional periodic potential," Nat. Commun. **4**, 1749 (2013).
[34] Y. V. Kartashov, V. V. Konotop, and V. A. Vysloukh, "Two-dimensional dissipative solitons supported by localized gain," Opt. Lett. **36**, 82 (2011).
[35] X. Ma and S. Schumacher, "Vortex-vortex control in exciton-polariton condensates," Phys. Rev. B **95**, 235301 (2017).
[36] V. E. Lobanov, Y. V. Kartashov, V. A. Vysloukh, and L. Torner, "Stable radially symmetric and azimuthally modulated vortex solitons supported by localized gain," Opt. Lett. **36**, 85 (2011).

[37]C. Huang, F. Ye, B. A. Malomed, Y. V. Kartashov, and X. Chen, "Solitary vortices supported by localized parametric gain," Opt. Lett. **38**, 2177 (2013).
[38]C. H. Tsang, B. A. Malomed, and K. W. Chow, "Multistable dissipative structures pinned to dual hot spots," Phys. Rev. E **84**, 066609 (2011).
[39]A. G. Vladimirov, J. M. McSloy, D. V. Skryabin, and W. J. Firth, "Two-dimensional clusters of solitary structures in driven optical cavities," Phys. Rev. E **65**, 046606 (2002).
[40]N. G. Berloff, M. Silva, K. Kalinin, A. Askitopoulos, J. D. Töpfer, P. Cilibrizzi, W. Langbein, and P. G. Lagoudakis, "Realizing the classical XY Hamiltonian in polariton simulators," Nat. Mater. **16**, 1120–1126 (2017).
[41]M. Nixon, E. Ronen, A. A. Friesem, and N. Davidson, "Observing geometric frustration with thousands of coupled lasers," Phys. Rev. Lett. **110**, 184102 (2013).
[42]G. Tosi, G. Christmann, N. G. Berloff, P. Tsotsis, T. Gao, Z. Hatzopoulos, P. G. Savvidis, and J. J. Baumberg, "Geometrically locked vortex lattices in semiconductor quantum fluids," Nat. Commun. **3**, 1243 (2012).
[43]V. Pal, C. Tradonsky, R. Chriki, A. A. Friesem, and N. Davidson, "Observing dissipative topological defects with coupled lasers," Phys. Rev. Lett. **119**, 013902 (2017).
[44]Y. V. Kartashov, V. V. Konotop, and V. A. Vysloukh, "Symmetry breaking and multipeaked solitons in inhomogeneous gain landscapes," Phys. Rev. A **83**, 041806 (2011).
[45]P. Hamel, S. Haddadi, F. Raineri, P. Monnier, G. Beaudoin, I. Sagnes, A. Levenson, and A. M. Yacomotti, "Spontaneous mirror-symmetry breaking in coupled photonic-crystal nanolasers," Nat. Photonics **9**, 311–315 (2015).